Chemical Geology 559 (2021) 119900

Contents lists available at ScienceDirect

Chemical Geology

journal homepage: www.elsevier.com/locate/chemgeo

Developing boron isotopes to elucidate shale weathering in the critical zone

Johanna Noireaux[a], Pamela L. Sullivan[b,*], Jérôme Gaillardet[a], Pascale Louvat[a], Grit Steinhoefel[c], Susan L. Brantley[d]

[a] Université de Paris, Institut de physique du globe de Paris, CNRS, F-75005 Paris, France
[b] College of Earth, Ocean, and Atmospheric Science, Oregon State University, Corvallis, OR 97331, United States of America
[c] Alfred Wegener Institute, Helmholtz Centre for Polar and Marine Research, Bremerhaven, Germany
[d] Earth and Environmental Systems Institute and Department of Geosciences, Pennsylvania State University, Univ. Pk, 16802, United States of America

ARTICLEINFO

Editor: Michael E. Boettcher

Keywords:
Critical Zone
Weathering
Boron
Shale
Isotopic Fractionation

ABSTRACT

To further develop boron isotopes as a tool for understanding shale weathering, we explored patterns of boron concentrations and isotopes across the forested Susquehanna Shale Hills Critical Zone Observatory (CZO). We present boron measurements for all watershed components that provided a foundation for examining water-rock interactions in a shale dominated watershed, including water compartments (e.g., precipitation, stream water, groundwater) and solid compartments (e.g., soil, bedrock, stream sediments, suspended load, and leaf litter). Results show boron isotopes ($\delta^{11}B$) in the bedrock (− 4.6‰) and soil (− 5.9 to - 4.2‰) were very similar. All waters were enriched in ^{11}B by comparison: precipitation (7.2 to 22.6‰), stream (10.3 to 15.5‰), and groundwater (2.2 to 17.4‰). Modeling revealed that isotopic fractionation observed in the surface water and groundwater could mainly be explained by water-rock interactions including clay mineral dissolution (e.g., chlorite) and coprecipitation/adsorption processes (e.g., coatings on illite particles), likely in the near surface soils (~2 m deep). We found that leaching, the loss of boron from vegetation to stream water, plays a secondary role. Specifically, such leaching likely contributes the equivalent of 10 to 26% of the B fluxes from the watershed outlet. Boron mass balance between bedrock and precipitation inputs and the exported flux of dissolved and solid pools identified a "missing" isotopically light solid flux ($\delta^{11}B$ of −12.2 ± 5.3‰ at ~4.4 ± 3.8 mol/ha/y of B; uncertainty reported as 2 SD). We did not sample any pool with this isotopic signature. Here our data suggest the composition of this pool is more likely related to precipitation of secondary clays rather than adsorption or (co)precipitation on Fe oxides. We propose two hypotheses to explain the missing light B pool: 1) a significant portion of the particles carrying the missing ^{10}B are not sampled because they enter groundwater at depth and are transported out of the catchment under the stream; and/or 2) the inputs and outputs of boron are not operating at steady state in the catchment today, suggesting that the missing boron particles were lost in the past in proportions higher than today. When this B budget is paired with studies of $\delta^{26}Mg$ and $\delta^{56}Fe$ from Shale Hills, both of which also show missing isotopic pools, the pattern indicates a fundamental gap in understanding of shale weathering. We concluded that light B particles, presumably generated in the upper soils, are likely transported deep beneath the surface in the groundwater system or episodically in the past through riverine fluxes.

1. Introduction

The critical zone (CZ) is the thin, near-surface zone of terrestrial Earth, where biological, hydrological, and chemical processes interlace. A major challenge in predicting how the CZ will respond to future climatic and anthropogenic pressures is the lack of quantitative relationships that describe how soils, vegetation, and rivers govern water and mass fluxes. Thus, we are charged with developing new proxies that can holistically describe these interactions. Often elements (e.g., Mg, Li, Si, Ca) and their isotopic compositions are employed to quantify processes (e.g., sorption/desorption, reincorporation, congruent/incongruent dissolution) governing mineral weathering fluxes at the watershed scale (e.g., see review in Sullivan et al., 2016a). In this paper, we continue to help transform boron isotopes into a tool that can be used to distinguish the controls of biological nutrient cycling and shale weathering processes on mass fluxes from a first order watershed.

Boron is unique compared to many other weathering isotopic proxies such as lithium or magnesium, which are not dominantly impacted by vegetation nutrient cycling (Millot et al., 2010a, 2010b; Schmitt et al., 2012; Opfergelt et al., 2012; Dellinger et al., 2015; Ma

* Corresponding author.
E-mail address: pamela.sullivan@oregonstate.edu (P.L. Sullivan).

https://doi.org/10.1016/j.chemgeo.2020.119900
Received 20 April 2019; Received in revised form 20 August 2020; Accepted 19 September 2020
Available online 28 September 2020

et al., 2015). Boron is 1) a micro-nutrient essential for biological growth, thus tightly recycled by vegetation (Power and Woods, 1997; Blevins and Lukaszewski, 1998, Brown et al., 2002, Broadley et al., 2012); and 2) a soluble element, likely to be released from minerals during continental weathering (e.g. review by Gaillardet and Lemarchand, 2018). Until recently, most studies have employed boron isotope fractionation as a tracer of anthropogenic contamination (Vengosh et al., 1994; Chetelat et al., 2005) or as a tracer of groundwater sources (Casanova et al., 2001; Mather and Porteous, 2001; Pennisi et al., 2006).

Globally, rivers are strongly enriched in ^{11}B compared to continental bedrock (Spivack et al., 1987; Lemarchand et al., 2000; Rose et al., 2000), a phenomenon attributed to: 1) boron derived from silicate weathering and then fractionated through water/rock interactions (e.g., Mackenzie river basin; Lemarchand and Gaillardet, 2006); 2) fractionation that occurs when boron is reincorporated into secondary phases, a process which favors ^{10}B incorporation, leaving the dissolved pool enriched in ^{11}B (e.g. Spivack et al., 1987; Chetelat et al., 2009a, 2009b; Cividini et al., 2010; Lemarchand et al., 2012, 2015); and 3) fractionation associated with the cycling of boron through vegetation, which can effectively impart an enriched signal to rivers as water interacts with vegetation (litter leaching or throughfall) (Cividini et al., 2010; Louvat et al., 2011; Louvat et al., 2014a, 2014b). Together these studies demonstrate that boron isotope fractionation is likely controlled by vegetation, climate, and lithology, underscoring the need to better constrain boron isotopes and their link to the processes controlling CZ evolution at the watershed scale. In this paper, we specifically focus on understanding what controls B weathering and solute fluxes from shale systems.

To elucidate boron isotope fractionation in upland systems, we examine boron isotopes at the Shale Hills subcatchment of the Susquehanna Shale Hills Critical Zone Observatory (SSHCZO), a 7.9 ha subcatchment underlain by the Rose Hill Shale. Shale is ideal for examining boron isotopic fractionation processes at the watershed scale because shale generally contains high concentrations of boron, e.g. 50 ppm to 200 ppm (Hu and Gao, 2008, Romer et al., 2014), and is dominated by incongruent weathering where B can be reincorporated into secondary phases fingerprinting the controlling geochemical processes. In addition, this research adds to the growing body of knowledge on boron isotope behavior at the catchment scale across climate and lithologic gradients (Cividini et al., 2010; Lemarchand and Gaillardet, 2006; Gaillardet and Lemarchand, 2018) by contributing a temperate climate shale catchment.

Shale Hills is an ideal site for understanding the boron system as the hydrology and geology of the watershed are well documented and numerous isotope tracers have been used to understand weathering processes and soil formation (e.g., U-series, ^{10}Be, Fe, Mg, S, C; Ma et al., 2010; Ma et al., 2013; Ma et al., 2015; Yesavage et al., 2012; West et al., 2013; Jin et al., 2014; Sullivan et al., 2016a), offering unprecedented constraint on data interpretation. Interestingly a puzzle has emerged from these multiple isotopic measurements at Shale Hills: isotopic fractionation between the bedrock, the stream, and the soils consistently suggest a "missing" reservoir. For example, mass balance on Mg isotopes (including measurements of stream water, groundwater, pore water, stream sediments and soils) showed that all pools were less than or equal to the isotopic signature of the bedrock ($\delta^{26}Mg = 0.36‰$), except one deep stream sediment sample which contained enriched $\delta^{26}Mg$. Ma et al. (2015) suggested that this might indicate an enriched pool was transported at some time in the past. The $\delta^{56}Fe$ data from Shale Hills also potentially suggests the loss of isotopically heavy Fe micron-sized particles from the system (Yesavage et al., 2012). Specifically, Yesavage observed a decrease in soil bulk Fe and HCl-extracted Fe isotopic ratios downslope with increasing weathering extent, which could be explained by Fe fractionation during precipitation on to particles not captured in the study. Finally, Noireaux et al. (2014) examined the depth profiles of soil mass transfer coefficients (τ) comparing concentrations of mobile and immobile elements in the weathered and parent material, and deduced that B was partly lost in the form of Al-bearing particles. Similar explorations in an almost identical, adjacent shale watershed revealed that roughly half of Mg and K depletion could be explained by particle loss from the soil (Hasenmueller et al., 2017) as had been previously suggested (Jin et al., 2010). Similarly, Kim et al. (2018) estimated that roughly half of the loss of some elements from the soils was by particle export from all depths. All together these data suggest that micron-sized particles with distinct isotopic and elemental composition have and may continue to be exported from this shale catchment. Although small amounts of particulates have been sampled, only one potential measurement of the "missing" pool has been identified (Ma et al., 2014), leading to the conclusion that this loss likely occurred in the past.

Here, our goal is two-fold. First, to further develop boron isotopes as a tool for elucidating critical zone processes (e.g., weathering and biotic cycling) in shale watershed catchments, and second, to ask the question, does the boron isotopic mass balance support the hypothesis that there is a significant proportion of micron sized particles leaving the watershed undetected. To address these goals, we measured boron isotope compositions and concentrations in the solid and dissolved load at the watershed scale, including precipitation, stream water, groundwater, litter, suspended particulate matter, soil, and bedrock. We then used these data to understand both the origins and processes controlling boron dynamics at Shale Hills and then solved a boron mass balance to determine if, indeed there is a missing pool in the isotope mass balance.

2. Material and methods

2.1. Hydrological and geological settings

Shale Hills is a 7.9 ha forested subcatchment of the SSHCZO located in central Pennsylvania (Fig. 1). The catchment is underlain by the Rose Hill Formation, which is primarily comprised of shale with thin carbonate- and quartz sand-rich interbeds located in the upper half of the stratigraphic section (i.e., near the outlet) (Flueckinger, 1969; Cotter et al., 1986; Sullivan et al., 2016b). The Rose Hill shale bedrock mainly consists of illite (~ 54 wt%), quartz (~ 33 wt%), and chlorite (~ 8.9 wt%), with trace amounts of pyrite, ankerite, and plagioclase feldspar (Jin et al., 2010). Here, pyrite and carbonates are weathered to the greatest depths (~23 m deep at the northern ridge top). At the termination of the zone of weathering of these minerals, chlorite begins to dissolve and continues to weather to the land surface (Gu et al., 2020). Closer to the land surface, the minor plagioclase component weathers away (~7 m deep at the northern ridge top) (Brantley et al., 2013). In general, the absolute depths of these reactions vary around the watershed (Gu et al., 2020). The bedrock is mantled by soil, defined here as the augerable regolith, that varies in depth from 30 cm at the ridgetop to > 180 cm in the valley floor (Lin, 2006).

Soils at Shale Hills are 100% depleted in pyrite and carbonate minerals (Brantley et al., 2013; Sullivan et al., 2016a, 2016b) and the weathering of illite (~3 m deep) and chlorite (~10 m deep) have resulted in the formation of kaolinite, vermiculite and hydroxyl-interlayered vermiculite (Jin et al., 2010). Quantitative X-Ray Diffraction (XRD) measurements indicate that the major minerals in the soils are quartz (~ 36–63 wt%), illite (~ 22–54 wt%), chlorite and vermiculitized chlorite (~ 3–9 wt%) and feldspar (~ 1.2–6.6 wt%) with trace amounts of Fe-oxides (~ 0–2.5 wt%) and kaolinite (~ 0–2.8 wt%).

Shale Hills is characterized by a temperate climate where the mean annual temperature and precipitation are 10 °C and 1100 mm, respectively (Thomas et al., 2013; Brantley et al., 2018). Precipitation inputs at Shale Hills are fairly constant over the year, but typically consist of snow in the winter (between December and March this represents 25% of the precipitation) and rain the rest of the year. During the summer, elevated rates of evapotranspiration result in extended no flow periods, where little to no discharge is observed from the first-order ephemeral stream. The average discharge at the catchment outlet between 2006 and 2010 accounted for 46% (509 mm) of the average annual precipitation. The catchment is dominated by temperate tree

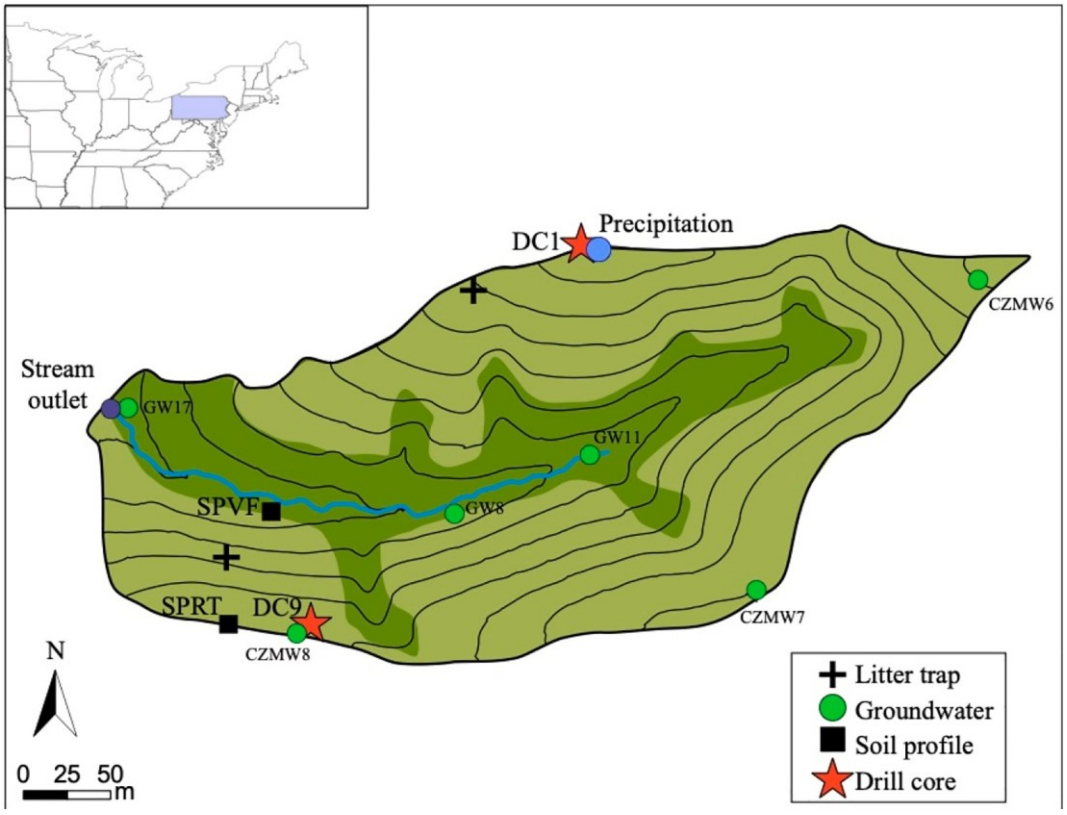

Fig. 1. Shale Hills, a subcatchment of the Susquehanna Shale Hills Critical Zone Observatory (CZO), is located in central Pennsylvania, USA (colored purple in inset). Boron sampling sites for water and solid materials are marked with symbols. CZMW8 is the same borehole (green symbol) where core material DC9 (red star) was recovered but they are plotted slightly offset for viewing. (For interpretation of the references to colour in this figure legend, the reader is referred to the web version of this article.)

species: deciduous oak (Quercus spp.), hickory (Carya spp.), maple (Acer spp.), evergreen hemlock (Tsuga spp.) and pines (Pinus spp.) (Smith, 2013).

2.2. Sample description

2.2.1. Bedrock, soils and sediment

Five bedrock samples from two cores (DC1 and DC9 (sampled in borehole CZMW8)), Fig. 1) drilled on the northern and on the southern ridgetops of the catchment were analyzed for boron isotopes and concentrations. Samples were analyzed from a depth of 6 m to 30 m. Precise descriptions of the DC1 core can be found in Jin et al. (2010) and Brantley et al. (2013), while DC9 can be found in Sullivan et al. (2016b).

Here we focus on two soil profiles located on the southern slope of the catchment (Fig. 1). The soil profiles define a transect from the ridge top (SPRT) to the valley floor at 5 m from the stream (SPVF) denoted as South Planar. Major element analyses for the same soils were previously reported by Jin et al. (2010). Boron concentrations and isotope ratios were measured on aliquots of the same soil samples and the results reported in Noireaux et al. (2014).

To characterize the particles lost from the erosion of the soils, we measured boron concentrations and isotopic composition on existing streambed sediment samples as well as newly collected suspended load material. Sediments from the streambed were collected at three locations; at 13 m and 60 m from the outlet, and the weir box located at the outlet. The two upstream sampling locations, labelled Sediments 13 m and Sediments 60 m (Table 2), were sampled and analyzed as bulk or sieved (< 2 mm) material at either 13 m or 60 m from the outlet. The weir box sediment ("Weirbox" in Table 2) was comprised of sediments that had accumulated for two years after the installation of the box. One sample (0–10 cm) from the sediment core located at a former weir (at the center of the valley; SSOW 0–10 in Table 2) and described in Ma et al. (2011) was also analyzed. Three new suspended load particulate samples were collected at the outlet from large volumes of stream water (10 l to 20 l) by vacuum filtration using 0.45 μm nylon filters. Samples were collected in spring and fall, when the largest flow events tend to occur. Particles were collected by removing material from filters by washing them with a small volume of Milli-Q water and then evaporating that water at low temperature (40 °C) until the particulate material was dry. These particles were then analyzed for B concentrations and isotopic composition.

2.2.2. Vegetation

Litter traps were located all over the catchment at 50 cm above the ground. The contents of two of these litter traps (Fig. 1) were collected in November 3rd 2012 (traps and litter described in Smith, 2013). Here, litter only included leaf material, not wood. Litter was then dried in a Binder Drying Oven at 57 °C for a minimum of 24 h. An aliquot of each trap content of about 100 mg was powdered in an agate mortar for boron analysis. Major element concentrations of litter were assumed to equal the average of the litter measurements reported by Herndon et al. (2015b).

2.2.3. Precipitation, stream water, and groundwater

Precipitation samples were collected on site by an automatic precipitation sampler (NSA 181S model, Eigenbrodt GmbH & Co., Germany) located in Shale Hills and with an open collector located in an adjacent open field (labelled "o.f.", 0.3 km southeast of the outlet). A total of 3 rain and 2 snow samples were collected in March 2013, October 2013 and in February 2014. Major element data for precipitation in 2013 and 2014 were obtained from two NADP sites (National Atmospheric Deposition Program), PA15 and PA42, located near the catchment (i.e., 22 km and 5 km, respectively).

Table 1
Chemistry of water (stream, ground and precipitation) collected at Shale Hills (2 std. dev reported).

	Date	B (ppb)	$\delta^{11}B$ (‰)	2 std. dev	pH	Ca (μM)	K (μM)	Mg (μM)	Na (μM)	Cl (μM)	NO3 (μM)	SO4 (μM)
Streamwater												
Streamwater 1	28/02/13	4.0	15.3	0.2	6.91	94	23	70	20	17	8	272
Streamwater 2	23/05/13	9.1	10.4	0.8	6.92	282	35	125	34	27		117
Streamwater 3	12/07/13	8.2	10.3	0.2	6.86	190	34	114	33	19	6	84
Streamwater 4	08/10/13	18.0	15.5	0.2		778	75	211	48			
Streamwater 5	11/10/13	11.0	15.1	0.3	6.07	245	41	203	149	43	1	141
Streamwater 6	21/01/14	5.8	13.6	0.3	8.34	146	23	84	25	18	4	91
Streamwater 7	17/02/14	8.0	11.6	0.2	7.78	167	27	135	41	25	6	114
Streamwater 8	13/03/14	4.5	14.5	0.2	7.41	80	21	61	16	21	6	80
Streamwater 9	21/03/14	5.0	15.1	0.8	6.43	230	25	158	111	21		95
Streamwater 10	28/03/14	4.9	11.9	0.1	5.69	199	24	94	32	19	8	95
Streamwater 11	01/04/14	4.6	13.8	0.2		157	26	113	86	16	5	
Streamwater 12	24/04/14	6.6	11.5	0.3	7.17	203	26	101	28	19	10	91
Streamwater 13	26/05/14	6.7	11.4	0.2	6.09	196	28	91	19	20	3	91
Streamwater 14	25/08/14	13.4	11.1	0.2	7.80	409	40	221	53			
Streamwater 15	13/09/14	14.8	10.5	0.4		606	41	199	60			
Groundwater (depth)												
GW08 (4 m)	08/02/13	3.0	17.4	0.2	7.50	281	24	70	20	104	8	115
GW11 (4 m)	08/02/13	4.0	16.4	0.2	6.98	139	28	71	19	26	7	94
GW11 (4 m)	10/09/13	6.2	13.8	0.5		81	31	96	38	26		85
GW17 (4 m)	08/02/13	8.0	5.7	0.2	7.59	1380	16	203	62	73	7	358
CZMW6 (8 m)	08/02/13	9.0	10.4	0.2	6.93	756	95	764	101	70	10	107
CZMW7 (8 m)	08/02/13	11.6	15.6	0.6	6.93	1880	81	870	680	82	7	273
CZMW8d (30 m)	23/05/13	82.0	2.2	0.2	7.28	368	23	571	500	77	5	168
Rainwater												
Rainwater 1	01/03/13	0.80	19.6	0.9	5.23[a]	1.9	0.7	1.3	4.5	4	16	9
Rainwater 2	07/10/13	7.20	10.6	0.3	5.56[a]	1.2	23.5	5.6	4.2	1	3	4
Rainwater 3 (open field)	11/10/13	0.20	22.6	1.9	5.84[a]	1.9	0.6	3.1	4.4	4	3	1
Rainwater 4	07/02/14	0.54	12.8	1.5	4.78[a]	2.6	0.7	0.8	0.9	8[a]	20[a]	8[a]
Rainwater 5	17/02/14	0.44	7.2	0.6	4.78[a]	6.5	0.5	1.2	2.1	11[a]	24[a]	17[a]

[a] Data from PA42 NADP station.

A total of 15 stream water samples were collected from the outlet of the catchment between February 2013 and September 2014. Each time, the volume that was collected was at least 250 ml. The groundwater samples (n = 7) were collected from six wells (GW08; GW11; GW17; CZMW6; CZMW7; CZMW8) that were 4 m to 30 m deep (Fig. 1, Table 1) located either in the valley or the ridgeline across the catchment. Stream water was collected manually, while groundwater was collected using a peristaltic pump. Three water samples were collected per event: one 120 ml acid washed Nalgene bottle for B analysis, and two 60 ml Nalgene bottles collected for anion and cation analysis. The samples for B analysis were syringe filtered using 0.45 μm nylon membrane and acidified with distilled concentrated nitric acid. The samples for anion and cation were filtered with a 0.45 μm polyethersulfone filter. Samples for cations were preserved with 3 drops of pure reagent grade nitric acid. Soil solutions were not collected as a part of this study as the porous ceramic suction cup lysimeters contain B and create contamination.

2.3. Boron concentration and isotopic measurements method

Boron concentrations of the water samples were determined by inductively coupled plasma mass spectrometry (ICP-MS), while for solids, boron isotope ratios and concentrations were measured by multi-collector-ICP-MS (MC-ICP-MS) after ion-exchange chromatography (details explained in Noireaux et al., 2014). The solids (soils, bedrock, river sediments, and litter) were first dissolved by K_2CO_3 alkali fusion following a modified version of the procedure by Chetelat et al. (2009a, 2009b). The sample-flux mixture (in a 1:7 weight ratio) was first heated at 950 °C in a furnace for 15 min. Then it was dissolved in a large volume (30–40 ml) of Milli-Q water, HNO_3 additions and ultra-sonication continued until the solution became clear, it was then ultra-sonicated for 1 h.

Boron was extracted from the solid samples in a three-step process. First, 4 to 8 ml of the fusion solution was introduced on a column containing 1 ml AGW50-X8 (Biorad) resin to retain the cations while the boron was collected with the efflux from the column. The resin was additionally rinsed with 6 × 500 μl HNO_3 0.1 M. The pH of the collected solution was increased to 8–9 by the addition of distilled NH_4OH. The resulting solution was introduced to a column with 50 μl of resin Amberlite IRA 743 that specifically retain B. The last purification step for the boron fraction was done on a column filled with 10 μl of resin Amberlite IRA 743. The wash and elution steps for these two columns are described in Paris et al. (2010), Louvat et al. (2010) and Louvat et al. (2014a, 2014b). For the water samples (stream water, precipitation, groundwater), boron was extracted using one column with 50 μl Amberlite IRA 743. The sample introduction volume was calculated for 300 ng B, based on the concentrations measured by ICP-MS, but limited to 50 ml.

The final boron solutions were then diluted to 0.05 N HNO_3 by addition of ultra-pure water. The boron concentrations were measured at the MC-ICP-MS (by comparison of the ^{11}B intensity of B standard solutions at 10, 50, and 200 ppb to the sample's ^{11}B intensity) before isotope ratio measurements, in order to match (within 10%) the standard and sample concentrations. The B concentrations of the solid samples were then back-calculated from these solution concentrations, by taking into account the mass of sample that was fused, the final volume of the fuse solution and the volume of sample that was introduced to the cationic column. Standard reference material JB2 was analyzed during the same sessions as the samples and the measured B concentration (24.3 ± 3.9 ppm, 2 std. dev, n = 6) showed good agreement with concentrations obtained by other methods (28.8 ± 1.5 ppm, 2 std. dev, n = 24, Michel et al., 2015). Another reference material for apple leaves (NIST 1515) was measured at 25 ppm B when the certified value is 27 ppm. Thus, yields for the boron extractions were considered complete (100%). Boron extraction blanks were 0.24 ± 0.17 ng B (n = 9) for the water sample protocol and 8.6 ± 2.5 ng B (n = 11) for the solid sample protocol.

At the Institut de Physique du Globe de Paris (IPGP), B isotope ratios were measured with an automated direct injection nebulization set-up for sample introduction (Louvat et al., 2010; Louvat et al., 2014a, 2014b), allowing for quicker wash-out times, lower instrumental blanks

and high sensitivity. Instrumental mass bias was corrected by standard-sample bracketing with NIST 951 standard reference material (Catanzero et al., 1970). B concentrations of the sample and bracketing standard solutions were adjusted within 10%. The long-term reproducibility of the measurements estimated on an in-house enriched standard was 0.20‰ over three years (Louvat et al., 2014a, 2014b). The accuracy of the measurements was regularly verified by measuring in-house standards (SE-43 = −43.29 ± 0.20‰) and international standards ERM-AE120, ERM-AE121 and ERM-AE122 (Vogl and Rosner, 2011) at −20.31 ± 0.19‰ (2 std. dev, n = 20), 19.55 ± 0.18‰ (2 std. dev, n = 60) and 39.34 ± 0.21‰ (2 std. dev, n = 20), respectively. The reproducibility of the boron measurements after extraction was better than 0.25‰ for the liquid samples and better than 0.6‰ for the solid samples. Repeated measurements of the JB-2 reference material gave 7.13 ± 0.55‰ (2 std. dev, n = 12), consistent with previously published measurements (Tonarini et al., 1997; Chetelat et al., 2009a, 2009b; Cividini et al., 2010; Wei et al., 2013).

2.4. Major element analysis

Major cations were analyzed by inductively coupled plasma-optical emissions spectrometer (ICP-OES PS300UV, Teledyne Leeman Labs, Hudson, NH). Anions were measured on a Dionex Ion Chromatograph (ICS-250; Sunnyvale CA). Major ion analysis had an analytical precision of ~3%.

3. Results

3.1. Bedrock, soils, and sediments

The shale samples from the two drill cores (DC1 and DC9) have $\delta^{11}B$ values and B concentrations that remained fairly constant with depth, averaging −4.6 ± 0.3‰ (2 std. dev, n = 5; Fig. 2; Table 2) and generally ranging between 74 ppm and 89 ppm (typical of marine shales; e.g., Hu and Gao, 2008). The only exception was the deepest sample on the north slope (DC1 ~24 m below land surface), previously identified as a carbonate-rich unit (Jin et al., 2010; Sullivan et al., 2016b), which had half the B concentration (37 ppm; Table 2). Consistent with this inference of high carbonate content in that sample, it also was observed to be enriched in calcium.

Soil $\delta^{11}B$ values were also fairly constant with depth at both locations. The two locations showed slightly different values however: $\delta^{11}B$ averaged −4.5 ± 0.3‰ in the valley floor soil (SPVF), similar to the bedrock, while at the ridgetop soil (SPRT) they were slightly more negative at −5.5 ± 0.4‰. Boron concentrations in soil at both locations were depleted compared to the bedrock (determined by normalizing boron to an immobile element, here Zr) (shown in Noireaux et al., 2014). Soil B concentrations at the ridgetop remained fairly constant (42 ± 1 ppm) with depth, while in the valley floor soil, B concentrations increased with depth (i.e., 59 ppm at the surface to 87 ppm at depth; Table 2).

Streambed sediments and the suspended particles showed similar $\delta^{11}B$ values (−3.3‰ and −4.7‰, respectively; Fig. 2) that were close to the bedrock value. The B concentrations in these two compartments (values ranged between 35 and 62 ppm) were on the lower end of what was observed in the soil/rock.

3.2. Vegetation

The two leaf litter samples (collected from two traps on 11/3/2012; see Fig. 1) had very different $\delta^{11}B$ values (13.4‰ and 4.9‰), and B concentrations (22 ppm and 34 ppm, respectively). These concentrations are consistent with published litter values worldwide but their isotope composition was lower than values (25‰ to 28‰) reported by Cividini et al. (2010) for a temperate granite catchment. Likewise, Gaillardet and Lemarchand (2018) reported a range from 39‰ to 50‰ in a tropical granite catchment.

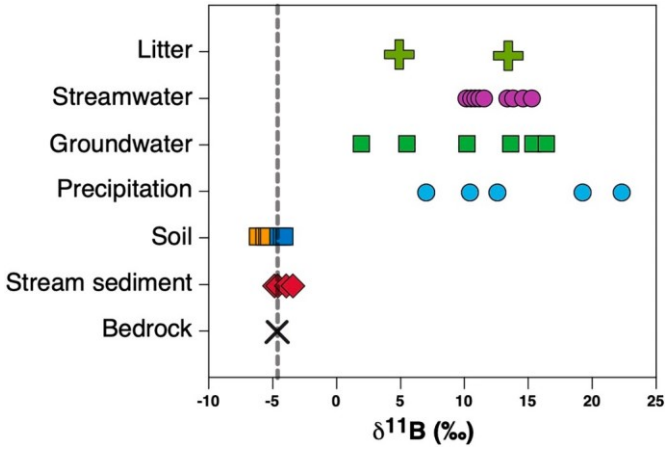

Fig. 2. Boron isotopic ratios in the litter (green cross), stream water (purple circles), groundwater (green squares), precipitation (blue circles), soil (squares; orange indicates ridgetop position and blue indicates valley floor position), stream sediment sediments and suspended load (diamonds), and the bedrock (X) at Shale Hills. (For interpretation of the references to colour in this figure legend, the reader is referred to the web version of this article.)

Table 2
Boron concentrations and isotopic composition of the soils, the bedrock, the sediments and the litter samples analyzed in this study.

		B (ppm)	$\delta^{11}B$ (‰)
Soils	Depth (cm)		
SPRT0010[a,b]	0–10	41	−5.5
SPRT1020[a,b]	10–20	43	−5.2
SPRT2030[a,b]	20–30	41	−5.9
SPVF0010[a,b]	0–10	59	−4.2
SPVF1020[a,b]	10–20	74	−4.6
SPVF3040[a,b]	30–40	71	−4.6
SPVF5060[a,b]	50–60	73	−4.9
SPVF6067[a,b]	60–67	87	−4.4
Bedrock (Drillcore)	Depth (m)		
DC1-26[a,b,c]	6	88	−4.4
DC1-36[a,b,c]	21	89	−4.5
DC1-38[a,b,c]	24	37	−4.7
DC9-39-40[d]	12	74	−4.6
DC9-100-101[d]	30	89	−4.8
Sediments			
Suspended load Spring		67	−4.5
Suspended load Fall		65	−3.8
Suspended load Fall		65	−4.8
Weirbox sediments[e]		58	−3.3
Sediments 60 m[e]		53	−4.2
Sediments 60 m (< 2 mm)[e]		62	−3.3
Sediments 13 m[e]		52	−4.3
SSOW 0-10[e]		52	−4.0
Litter (littertrap n°)	Date		
SHL #54	03/11/12	34.0	4.90
SHL #8	03/11/12	22.0	13.40

[a] Boron data are from Noireaux et al. (2014).
[b] Bulk chemistry in Jin et al. (2010).
[c] Bulk chemistry in Brantley et al. (2013).
[d] Bulk chemistry in Sullivan et al. (2016b).
[e] Bulk chemistry in Ma et al. (2011).

3.3. Precipitation, stream water and groundwater

In general, B concentrations at SSHCZO were lowest in the precipitation (0.2–7.2 ppb) and increased in the stream water and groundwater (Fig. 3). The precipitation collected in the open field collector showed a lower B concentration than the precipitation collected on-site (under the canopy) during the same period. Generally the B concentrations in the precipitation were consistent with the 0.8 ppb average (30 precipitation samples) from the Strengbach basin (Cividini et al., 2010) but are at the

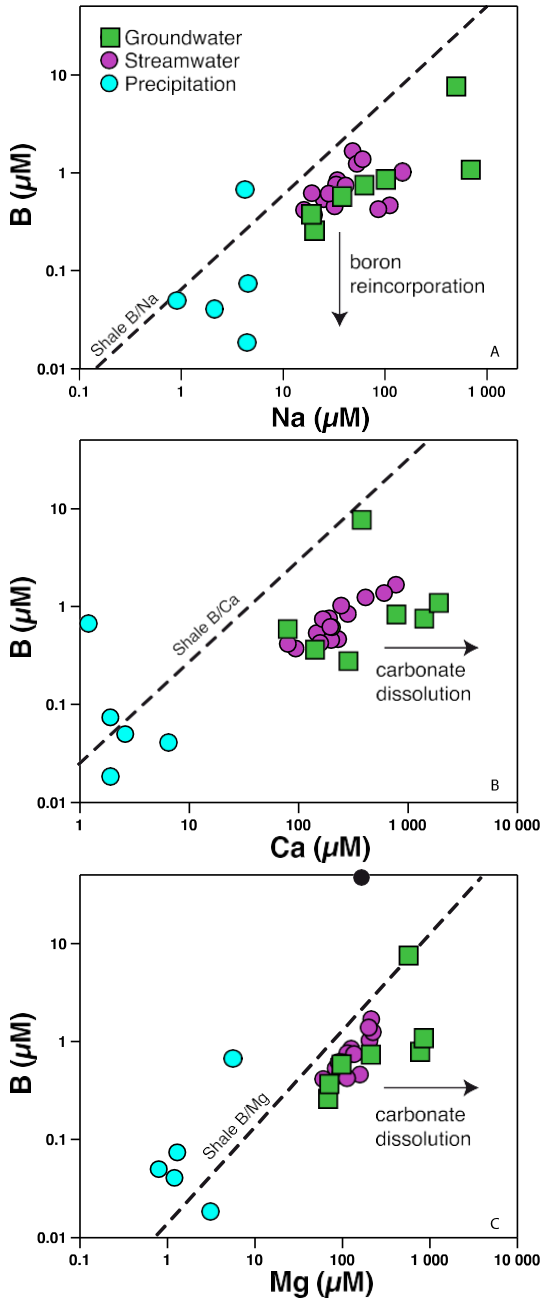

Fig. 3. Boron vs Na, Mg, and Ca concentrations in the precipitation (blue circles), stream water (purple circles), and the groundwater (green squares). Dashed lines represent the average element ratios for the bulk shale measured in this study. Carbonate dissolution and B adsorption are processes that could be modifying the B to Na, Ca and Mg ratios from rocks or precipitation as shown with arrows. (For interpretation of the references to colour in this figure legend, the reader is referred to the web version of this article.)

low end of the range (0.1–67 ppb) compared to other continental precipitation values (Chetelat et al., 2005; Mather and Porteous, 2001; Park and Schlesinger, 2002; Rose-Koga et al., 2006, Roux et al., 2017).

Concentrations of major elements (Na, Mg, and Ca) in the waters at Shale Hills were similar in pattern to B in that their concentrations were elevated in the stream water and groundwater compared to that of the precipitation. When element / B ratios were compared, stream and groundwater chemistry often showed a greater ratio compared to the precipitation, indicating potential chemical weathering processes (e.g., adsorption, carbonate dissolution) that act to change the stream water and groundwater solute concentrations.

The $\delta^{11}B$ value of the water samples ranged from 2.2‰ to 22.6‰ with the greatest range observed in the precipitation (7.2–22.6‰), followed by the groundwater (2.2–17.4‰), and the lowest range was measured in the stream water (10.4–15.5‰) (Fig. 2). The large range of $\delta^{11}B$ in precipitation at a single location is not surprising and has also been observed at several locations in France, with the annual variations at a single sampling site as high as 33‰ (Millot et al., 2010a, 2010b; Roux et al., 2017). While the highest $\delta^{11}B$ values for the water samples were observed in the precipitation, the lowest were observed in the groundwater, with the deepest well (~ 30 m below ground surface) representing both the highest B concentration and the lowest $\delta^{11}B$ value (Table 2). Finally, the isotopic composition of the stream (10 to 15‰) was within the range of previously published isotope ratios for large rivers in a temperate climate (Lemarchand et al., 2000; Rose et al., 2000) and in agreement with the general ^{11}B-rich nature of river waters.

4. Discussion

The isotopic measurements at SSHCZO document that critical zone pools in a small watershed can show large differences in $\delta^{11}B$ values (e.g., bedrock, soils and sediments between −6 and −3‰, groundwaters between +2 and +17‰, precipitations between +7 and +23‰, and litter at +5 to +14‰). We infer therefore that B isotope ratios and B isotope concentrations can be a good tool for understanding processes governing watershed evolution such as chemical weathering, flow path generation, and nutrient cycling. The pattern that emerges from these data is that the bedrock and soil have a very similar, isotopically light composition, while all other CZ compartments (e.g., waters, vegetation) all have isotopically heavier $\delta^{11}B$ compositions. Below we first explore the origin and processes controlling B at Shale Hills and then estimate B fluxes and finally derive a mass balance to explore if small particle fluxes represent an important but unsampled isotopic weathering flux in this shale catchment.

4.1. Origin and processes controlling boron

4.1.1. Sources of boron delivered in precipitation

Multiple sources of boron can be invoked to explain the large variability in the observed $\delta^{11}B$ values of precipitation at Shale Hills (Fig. 2). For example, potential sources include seasalts, biomass burning, anthropogenic emissions from industries, fertilizers spreading and fossil-fuel burning (Park and Schlesinger, 2002). The comparison of $\delta^{11}B$ to NO_3/B ratio (Fig. 4) suggests that most of the precipitation collected at Shale Hills is a mixture between two end-members: seawater (high $\delta^{11}B$ and low NO_3/B ratio; $\delta^{11}B$ > 39.6‰ and NO_3/B ~ 0) and anthropogenic emissions (low $\delta^{11}B$ and high NO_3/B ratio). Anthropogenic nitrate inputs to Shale Hills have occurred over the last several decades (Weitzman and Kaye, 2018).

Here, low $\delta^{11}B$–high NO_3/B ratio precipitation was collected during the winter time and may be associated with anthropogenic activities such as fossil-fuel burning which produces nitrate. We rule out activities such as fertilizer spreading and biomass burning as the source because neither activity is important in the winter, and we have no knowledge of fertilizer use in the catchment. The samples enriched in NO_3 are also enriched in SO_4 (Table 1). High nitrate and sulfate concentrations are consistent with coal burning emissions that are occurring in central Pennsylvania (Davidson et al., 2005). Fly ash leachates collected in several coal fired power plants in the U.S. have an average $\delta^{11}B$ of −6‰ (Ruhl et al., 2014), which is consistent with $\delta^{11}B$ of one of our endmembers (see anthropogenic emission Fig. 4). This is also consistent with the anthropogenic sources of B in rainwater identified in Guiyang, China (Zhao and Liu, 2010) and in Paris, France (Chetelat et al., 2009a, 2009b) which also had high NO_3/B ratios (> 400) and low $\delta^{11}B$ values (+5‰ and −20‰, respectively).

The precipitation sampled at SSHCZO, derived from a sampler in a clearing along the ridge, generally had an isotopic composition similar

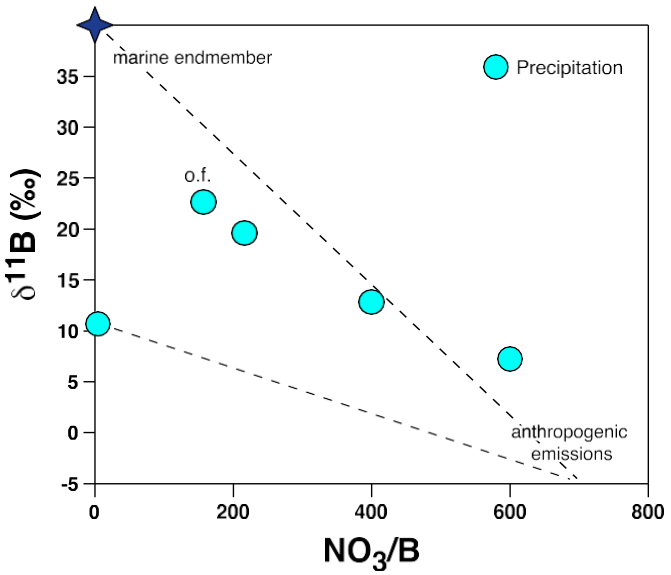

Fig. 4. Correlations between $\delta^{11}B$ and the NO_3/B (mol/mol) in precipitation. Here, inputs from two end members (sea/marine water (SW) and anthropogenic emissions) can generally explain the chemistry of the precipitation. The sample collected in the open field, designated by "o.f.", also falls along the mixing line whereas the one sample that falls off the line is attributed, by inference, to inputs from vegetation.

to that of precipitation from an adjacent open field (labelled "o.f."; Fig. 4). Thus, the precipitation was consistent with little interaction with trees before sampling. However, one precipitation sample showed low NO_3/B and a relatively low $\delta^{11}B$. This low NO_3/B-low $\delta^{11}B$ sample also exhibited high concentrations of K and Mg, and showed low concentrations of Na, all of which are common in samples that have interacted with vegetation. We infer that this sample was not representative of the precipitation input at Shale Hills but rather was influenced by biologically-cycled boron. Unfortunately, we were unable to sample throughfall so as to test this explicitly. In the literature, the limited number of observations of throughfall made on $\delta^{11}B$ has shown values ranging from similar to that of vegetation and higher (i.e., Cividini et al., 2010).

In summary, a first order explanation of B in precipitation at Shale Hills is that it is controlled by inputs from marine origins and anthropogenic emissions. In view of the variety of boron sources and isotope composition of these sources, it is difficult to infer an average composition of precipitation. Thus, when determining mass balance (below) the contribution of boron from precipitation was calculated at the annual scale.

4.1.2. Mineral dissolution

Given that precipitation processes do not completely explain the observed B concentrations and isotopic ratios in the stream and in the groundwaters (Table 1 and Fig. 2), we next explore the impact of mineral dissolution focusing on two major groups of bedrock minerals: carbonate and silicate minerals.

At Shale Hills, both calcite ($CaCO_3$) and ankerite ($(Ca,Mg,Fe)CO_3$) are observed at depth and could contribute Ca and Mg and dissolved inorganic carbon to groundwater and stream water (Jin et al., 2011, 2014), significantly increasing calcium and magnesium ion concentrations. Yet, the B isotopic ratios and concentrations presented above indicate that ankerite dissolution does not greatly affect the B solute budget. Specifically, the DC1 drill core sample taken from an interval at 24 m deep, where the parent material is enriched in carbonate minerals, has roughly half the B concentration compared to the other drill core samples but the same $\delta^{11}B$. This pattern indicates that the presence of carbonate has little to no effect on the $\delta^{11}B$ value of the bedrock, and is consistent with the low partitioning coefficient of B in inorganic carbonate. In addition, two groundwater samples were likely impacted by carbonate dissolution (e.g., Fig. 3; Ca concentrations > 1300 μmol), yet B concentrations showed no consistent increase. Assuming a maximum B concentration in carbonates of 5 ppm, the B/Ca ratio in carbonate minerals is estimated to be about 5×10^{-5} (mol/mol). Assuming that Ca in the stream originates only from carbonate dissolution, the maximum boron contribution from carbonates is 2.5%. We thus neglected carbonate dissolution as a source of B to the stream. The lack of contribution from carbonate dissolution to the dissolved boron budget is consistent with the conclusions inferred from the B chemistry of another watershed, i.e., the Changjiang (Chetelat et al., 2009a, 2009b).

In addition to ankerite, the Mg silicate minerals (illite and chlorite) also dissolve and affect the stream water solute chemistry at Shale Hills. For example, high Mg concentrations have been observed during low stream discharge and have been attributed to the combined dissolution of carbonates and clay minerals (Jin et al., 2011). The $\delta^{13}C$ values from the stream water and groundwater at Shale Hills also lead to the inference that the water chemistry is controlled by both silicate and carbonate mineral dissolution (Jin et al., 2014). The low $\delta^{11}B$ values observed in the groundwater data from the deep ridgetop well (CZMW8) show clear evidence of shale dissolution as this value is similar to that of the rock (Table 1). The only other location with low $\delta^{11}B$ values was observed in a shallow well near the outlet, an area known to be affected by mixing of waters characterized by short- and long-residence times that could include solutes released from chlorite weathering (Sullivan et al., 2016b). In addition, stream water chemistry at low discharge also showed low $\delta^{11}B$, consistent with solute contributions from dissolution of shale minerals (Fig. 5).

4.1.3. B adsorption and reincorporation in secondary minerals

The reincorporation or adsorption of B on clay minerals, organic particles, and mineral surfaces is known to strongly fractionate boron isotopes and to cause the enrichment of ^{11}B signatures in solutions. This process has specifically been invoked to explain the high $\delta^{11}B$ in several streams and large rivers (Chetelat et al., 2009a, 2009b; Lemarchand et al., 2015; Williams et al., 2001; Rose et al., 2000; Gaillardet and Lemarchand, 2018). In the soils at Shale Hills, depletion of major elements (Jin et al., 2010) and geochemical modeling (Sullivan et al., 2019) indicate that clay formation and transformation occur. According to classical interpretation, water rock interactions are two-step reactions where minerals first dissolve and then new mineral phases precipitate, incorporating elements such as Al, one of the least soluble elements in soils. During this mineral transformation, Na is not significantly reincorporated or adsorbed in secondary minerals and can therefore be used as a reference against which the behavior of other elements can be compared. B incorporation or adsorption on secondary minerals can explain the fact that groundwater and stream water have lower B/Na ratios compared to shale (Fig. 3) and that these waters have higher $\delta^{11}B$ compared to the shale. Thus, the difference between the B/Na ratio of the water and that of the rock is attributed to B loss during reprecipitation or adsorption. To quantify the loss, we define the fraction of boron left in solution, f_B, as (Fig. 5):

$$f_B = \frac{\left(B/Na\right)_{dis}}{\left(B/Na\right)_{rock}} \quad (1)$$

where $(B/Na)_{dis}$ is the ratio of dissolved B to Na in water (e.g., stream water and groundwater) and $(B/Na)_{rock}$ is that of the rock. The $(B/Na)_{rock}$ ratio (mol/mol) was measured as 0.07 ± 0.01 for the shale sampled above the ankerite-rich layer, while the B/Na ratio of the deeper ankerite-rich shale endmember was 0.03. We applied the ankerite B/Na_{rock} ratio when groundwater samples had Ca concentrations greater than 300 μM, as these concentrations have been attributed to ankerite-water interactions (Jin et al., 2014). The calculated values of f_B

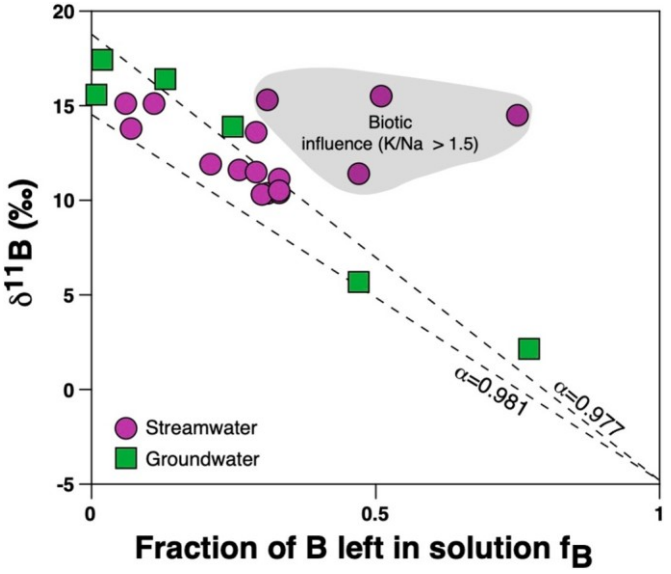

Fig. 5. Stream water (purple circles) and groundwater (green squares) $\delta^{11}B$ composition and f_B (the fraction of boron left in solution) compared to open flow-through model predictions (based on two potential fractionation factors $\alpha_{sec-dis}$ of water-rock interactions, see Eq. (3)). (For interpretation of the references to colour in this figure legend, the reader is referred to the web version of this article.)

vary from almost 0 (100% of B released to solution was subsequently re-precipitated) to about 0.8 (20% of released boron reincorporated into secondary phases).

It is possible to model the isotopic effects produced by these water-rock interactions using an open flow-through modeling approach (Eqs. (2), (3); Bouchez et al., 2013; Dellinger et al., 2015), assuming in this case that Na is conservative (meaning once dissolved it remains in solution). In this model, the bedrock is first dissolved and then B is fractionated between the secondary minerals and the residual water. While simple in formulation, Bouchez et al. (2013) has demonstrated that such a flow-through model can be successful in predicting isotopic compositions of waters (soil, ground, stream) for Li, B, Mg, Si and Ca isotopes in over 500 samples from ~50 sites. Outlined below is the flow-through model for B where the isotopic composition of the dissolved boron is noted as $\delta^{11}B_{dis}$ and that of the secondary clay or adsorbed B as $\delta^{11}B_{sec}$:

$$\delta^{11}B_{sec} = \delta^{11}B_{dis} + \Delta_{sec-dis} \quad (2)$$

$$\delta^{11}B_{dis} = \delta^{11}B_{shale} - (1 - f_B) \times \Delta_{sec-dis} \quad (3)$$

Here, $\Delta_{sec-dis} = \delta^{11}B_{sec} - \delta^{11}B_{dis}$ ($\approx 1000 \times \ln \alpha_{sec-dis}$) the isotopic fractionation between the secondary phases and the dissolved load, and $\alpha_{sec-dis}$ represents the fractionation coefficient between secondary phases and the dissolved load. Depending on the complex formed at the mineral surface and the crystallographic structure of the newly formed minerals, $\Delta_{sec-dis}$ can show very large variations ranging from −60‰ to 1‰ (Lemarchand et al., 2007). However, from the experimental work published so far, the overall observation is that light B is preferentially incorporated on mineral surfaces and in solids (Palmer et al., 1987; Rose et al., 2000; Lemarchand et al., 2007).

Fig. 5 shows that except for a few samples (to be discussed separately), all stream water and groundwater samples plot along a linear trend best explained by a flow-through model and $\alpha_{sec-dis}$ values between 0.981 and 0.977 (20‰ and 23‰). This range of values is consistent with what has been published so far for the fractionation of boron incorporated into or adsorbed on clay minerals (Palmer et al., 1987; Lemarchand and Gaillardet, 2006; Gaillardet and Lemarchand, 2018) rather than into or on iron oxides (Lemarchand et al., 2007) over the range of pH found in Shale Hills. In comparison, the model fit for a Rayleigh distillation approach using reasonable fractionation factors was poor (see supplemental material).

What emerges from this analysis is that groundwater and most stream water (except samples with K/Na > 1.5) are consistent with the interpretation that adsorption or incorporation of boron on or in clay minerals adequately explains the B isotopes and concentrations. This furthermore suggests that the stream is largely impacted by water-rock interaction processes within the soil where formation of secondary minerals and adsorption of boron is most likely to occur and also in the groundwater (rock dissolution) (Fig. 5). This is consistent with hydrologic interpretations of large inputs of interflow (fast subsurface groundwater flow in the upper 5–8 m) and some influxes of deeper, regional groundwater into the stream at Shale Hills (Sullivan et al., 2016b; Brantley et al., 2017). The relatively high $\delta^{11}B$ stream values plotted on the flow-through model line (Fig. 5) require that at least 70% of the boron was reincorporated into secondary products during weathering. Given that the soil profiles in Noireaux et al. (2014) show that B is lost concomitantly with Al, Fe, Mg and K from the soil profile, a signature of particle loss, we infer that B loss occurs to a greater degree in near surface soils than at depth. Yet, isotopic pools of bedrock and soil reservoirs are fairly similar, which suggests that partitioning of light B is likely as a precipitated coating on these small particles.

4.1.4. Vegetation leaching

Although clay dissolution and adsorption processes can explain the majority of data, four surface water samples fall outside of the flow-through model predictions (Fig. 5). These four samples not only have high $\delta^{11}B$ (compared to their B/Na ratio) and high B concentrations, they also contain elevated concentrations of K and Mg (Table 1). Several studies have shown that vegetation and throughfall (precipitation that interacts with vegetation on its way to the ground) are enriched in B and in ^{11}B. Throughfall often shows a $\delta^{11}B$ signature that can be 10‰ higher than that of the precipitation (Chetelat et al., 2009a, 2009b; Gaillardet and Lemarchand, 2018). In addition, we know vegetation is also enriched in K and Mg (e.g., Herndon et al., 2015b). We interpret the $\delta^{11}B$ signature of the samples that lie out of the predicted flow-through model to be influenced by biotic interaction. We propose that the high K and B concentrations in these stream samples indicate differences in dominant flow paths contributing to the stream at Shale Hills. When the K/Na ratio of the stream water is high (> 1.5), it reflects a dominant contribution of shallow flow paths of water through the hillslopes. These flowing waters have interacted with vegetation via throughfall and/or leaching of litter. In contrast, low K/Na ratios indicate deeper water flowpaths that experienced a lesser degree of interaction with vegetation or were overprinted by longer interaction times in the subsurface. High frequency stream water solute concentrations from Shale Hills between 2007 and 2010 (Herndon et al., 2015a) show that the K/Na ratio only exceeds this 1.5 threshold ratio 10% of the time. In contrast, we observed samples with high K/Na in as many as 26% of our stream water samples. The Mule Hole watershed in India is an extreme example of this same type of shallow flow path behavior that can control stream water chemistry: in Mule Hole, the B concentration in stream water under high flow mirrors that of the throughfall and litter (Gaillardet and Lemarchand, 2018). Interestingly, inputs of vegetation leaching to the stream at Shale Hills are not correlated with stream discharge or season.

4.2. Boron budget at the watershed scale

A simple interpretation of Fig. 2 is that one important component depleted in $\delta^{11}B$ has not been sampled at Shale Hills. Specifically, we would have expected to measure a pool more depleted in ^{11}B than the parent rock (~ −5‰) given that stream water, groundwater, sediments, soils and vegetation were either the same or enriched compared to the parent material. To have created such an enriched pool through

weathering and biological cycling by vegetation means some light pool was not measured. Below we use a mass budget approach to calculate the missing sink at steady state.

4.2.1. Atmospheric and vegetation controls on dissolved B fluxes

Atmospheric estimates of B delivered to Shale Hills were determined using measured average annual B fluxes. In the absence of significant dry deposits, the incoming B fluxes to the catchment are brought by precipitation. The boron fluxes into and out of the catchment, $F_{B,precip}$ (mol/ha/yr) and $F_{B,stream}$ (mol/ha/yr), are thus calculated using the mean annual precipitation (P; m/year) and mean annual discharge fluxes from the stream (Q; m^3/year), respectively. These are multiplied by the precipitation- (P_i; m/year) and discharge- (Q_i; m^3/year) weighted boron concentrations from the collected sampling events (i):

$$F_{B,precip} = A \times P \times \frac{\sum P_i \times [B]_{precip,i}}{\sum P_i} \quad (4)$$

$$F_{B,stream} = \frac{Q}{A} \times \frac{\sum Q_i \times [B]_{stream,i}}{\sum Q_i} \quad (5)$$

We used the 2006–2014 average precipitation (P = 1.08 m/year) and the average of the 2006–2010 discharge (Q = 38,400 m^3/year) data measured at the Shale Hills catchment (Duffy, 2012, 2013). To determine the fluxes (A = area = 7.9 ha), we assume that P is uniform across the site, and that Q represents the entire discharge from the catchment. The discharge-weighted concentration of B was 0.56 μmol/l and the precipitation-weighted concentration of B was 0.10 μmol/l. Using these values we calculated $F_{B,stream}$ at 2.8 ± 1.1 mol/ha/yr and $F_{B,precip}$ at 0.7 ± 0.2 mol/ha/yr (uncertainty was calculated as square root of the sum of the partial derivatives of the variables multiplied by the uncertainty of each variable squared). Thus, $F_{B,precip}$ represents 25 ± 12% of the stream boron flux. We then corrected the total boron exported by the stream for atmospheric deposition and arrived at an $F_{B,stream}$ of 2.1 ± 1.3 mol/ha/yr. We did not use typical atmospheric conservative tracers to further constrain atmospheric B inputs given that additional sources of Cl have been reported to contribute to the stream water at Shale Hills (Li et al., 2017) and Na and SO_4 are generated by weathering of shale and pyrite. The use of SO_4 is further compounded by historic loading associated with acid rain. Based on flow-through model results it is also important to note that $F_{B,stream}$ represents, to some degree, B "leaking" from the vegetation to the watershed, which elevates the B concentrations (in ~26% of the sampled events). At Shale Hills, this vegetation "leaking" of B only has a substantial impact on the concentration of B observed in the stream and not on the $\delta^{11}B$ as demonstrated by the similar isotopic composition of the litter and stream water (Fig. 2) and stationary isotopic composition of the "biotically influenced" stream water samples, which deviated away from the predicted flow through model (Fig. 5).

In summary, we have estimated that the total B flux exported by the stream after correction for atmospheric input is 2.1 ± 1.3 mol/ha/yr and that the annual B precipitation flux represents 25 ± 12% of the stream boron flux. Assuming that precipitation has an average $\delta^{11}B$ of 15.5‰ (excluding the precipitation sample influenced by throughfall), we estimate that the average stream $\delta^{11}B$ decreases from 12.8‰ to 11.4‰ once corrected for atmospheric inputs.

4.2.2. Bedrock denudation

To estimate the contribution of bedrock weathering to the boron budget at the catchment scale, we used the range in published soil production rates, Sp, for the catchment (17 m/Myr to 52.4 m/Myr by U-series; Ma et al., 2010, 2013) estimated at soil profiles in Shale Hills including SPVF and SPRT. To estimate the B flux associated and account for the variability in the Sp coming from the bedrock, $F_{B,D}$, we derived an area-weighted Sp for the watershed based on the reported Sp values for three (j) areas (A) (i.e., valley floor, midslope, and ridge top area in the watershed) obtained by Ma et al., the B content of the bedrock, $[B]_{rock}$, and the rock density, ρ_{rock}:

$$F_{B,D} = [B]_{rock} \times \rho_{rock} \times \frac{\sum Sp_j \times A_j}{\sum A_j} \quad (6)$$

Here $[B]_{rock}$ is 88 ppm (Noireaux et al., 2014) and ρ_{rock} is 2.6 g cm^{-3} (Ma et al., 2013). The overall area-weighted average denudation rate for the catchment was 31.9 m/Myr, which provided an estimate of $F_{B,D}$ of 6.5 ± 3.5 mol/ha/yr, a value more than three times higher than the dissolved B flux exported by the stream.

4.2.3. Boron export as solid material

At the watershed scale, we consider that the soils at Shale Hills are at an approximate steady-state, which is in agreement with the soil production and denudation rates estimated by U-series isotopes (Ma et al., 2010, 2013) and ^{10}Be (West et al., 2013), respectively. When we assume steady-state, all the boron produced by chemical weathering reactions must leave the watershed either as a dissolved component (< 0.45 μm) or as a solid component (≥ 0.45 μm). At Shale Hills, this exported solid phase consists of newly formed secondary particles (e.g., neoformed clays; Jin et al., 2010) as well as coatings on primary clay particles (e.g., illite) (Herndon et al., 2018; Kim et al., 2018), which have been observed on colloids extracted from soil water and groundwater samples. Based on the steady state hypothesis, we calculated the flux of solid B needed to close the mass budget:

$$F_{B,D} = F_{B,exported\ solid} + F_{B,stream} \quad (7)$$

Using $F_{B,D}$ of 6.5 ± 3.5 mol/ha/yr (Section 4.2.2) and $F_{B,stream}$ of 2.1 ± 1.3 mol/ha/yr (Section 4.2.1) we estimated that the solid exported flux of B, $F_{B,exported\ solid}$, was 4.4 ± 3.8 mol/ha/yr at Shale Hills using Eq. (7) (Fig. 6). Despite the large uncertainties associated with these fluxes, the main message revealed by this calculation is that most of the boron (70%) is leaving the watershed in a solid form. If we take an average concentration of 60 ppm B for river sediments (Table 2), and use the published values of exported solid fluxes at Shale Hills (erosion rates of 15–19 m/Myr, Jin et al., 2010 and West et al., 2013), then we can estimate that 2.2–2.7 mol/ha/yr of B is exported in a solid form at Shale Hills. This flux based on erosion rates is low but within error of our mass budget estimate of 4.4 ± 3.8 mol/ha/yr.

Given our estimates of both $F_{B,D}$ and $F_{B,stream}$, the mass balance approach also constrains the isotopic composition ($\delta^{11}B_{exported\ solid}$) of the exported solid flux ($F_{B,exported\ solid}$) in the B budget:

$$F_{B,D} \times \delta^{11}B_{rock} = F_{B,exported\ solid} \times \delta^{11}B_{exported\ solid} + F_{B,stream} \times \delta^{11}B_{stream} \quad (8)$$

We found that a $\delta^{11}B$ value of −12.2 ± 5.3‰ for the exported solid flux of boron was necessary to close the isotopic mass budget. However, the measured $\delta^{11}B$ of the stream suspended load (−4.2‰), streambed sediments (−4.0‰), and the soil profiles (−5.0‰) show almost no fractionation with respect to the bedrock composition (−4.6‰; Table 2) and are 5‰ to 6‰ higher than this estimated particle $\delta^{11}B$ (Fig. 6). While the mass budget and erosion rate estimates for $F_{B,exported\ solid}$ agree within error, the isotopic budget reveals that isotopically light B is clearly missing at the Shale Hills CZO.

4.3. How is Shale Hills losing light B?

Our data suggest that two processes govern the isotopic composition of B: vegetation cycling and rock-water interactions (clay dissolution and precipitation and/or absorption). But the data also are consistent with a missing pool and flux of light B at Shale Hills. There are very few data available on the different plant tissues but recent studies suggest that important isotopic fractionation occurs between the leaves, exudates and wood in trees (Cividini et al., 2010; Geilert et al., 2015; Geilert et al., 2019). The two latter studies reported that wood tissues were 24 to 27‰ lower that leaves in different plant species. With the

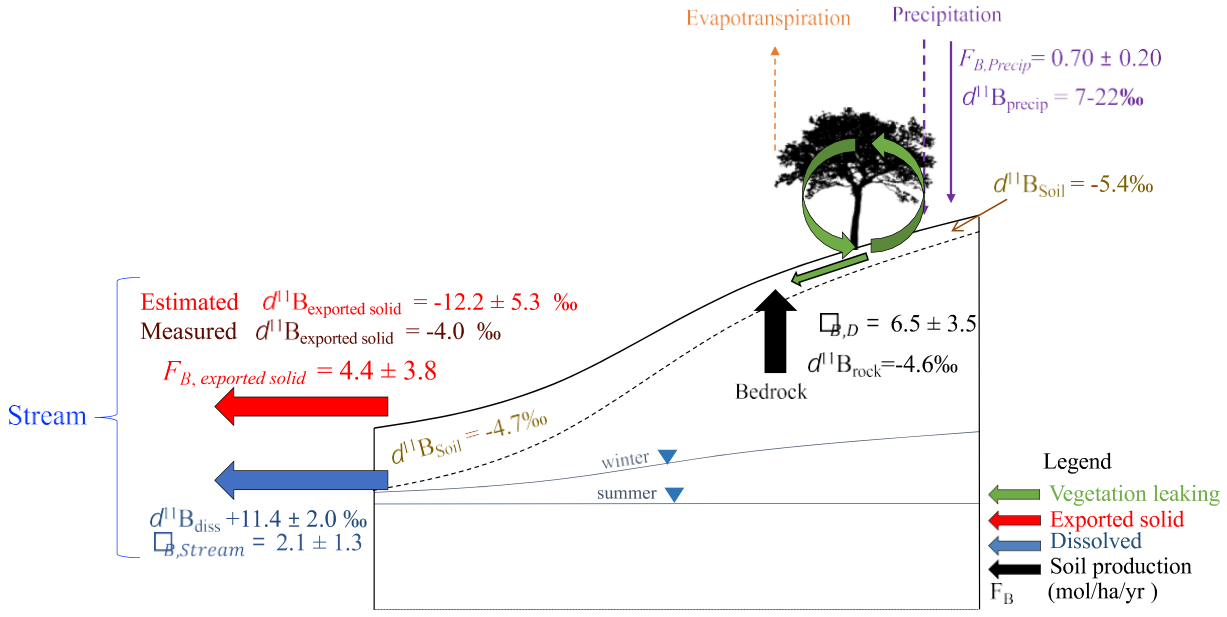

Fig. 6. Annual mass balance of boron in the Shale Hills watershed. Boron fluxes (F_B; mol/ha/yr) and isotopic composition ($\delta^{11}B$; ‰) associated with precipitation (purple), soil production from the bedrock (black), and stream water export of dissolved species (blue) and solid material (dark red), in addition to the B isotopic composition of the soil (brown). The mass balance revealed a missing isotopically light B flux, and we attributed this to exported solid material not sampled nor measured for isotopic composition (bright red). The estimated $\delta^{11}B$ of the exported solid material lost at Shale Hills was substantially lighter than the $\delta^{11}B$ measured in the suspended or bedload material (dark red), soil (brown), or even bedrock (black). (For interpretation of the references to colour in this figure legend, the reader is referred to the web version of this article.)

litter measured here between 5 and 15‰, this would mean that tree wood would be as low as −10 and −20‰, consistent with the range of isotopes that should be in the missing boron. As we did not measure boron isotopes in the tree wood, we cannot rule out that isotopically light B might be stored in the wood, but two arguments run against this hypothesis. First, we expect that over long periods of time most of the woody debris decays within the catchment; thus, the B pool is retained within the system and therefore does not support the missing flux of B. Second, it seems difficult to reach the necessary flux of missing boron (4.4 mol/ha/yr) by exporting wood fragments from the catchment.

We conclude from the stream water data that water-rock interactions (rather than vegetation) mainly control the behavior of B and thus, the missing light boron pool. Based on the above calculated value of $\delta^{11}B$ of the missing B pool at steady state (−12‰), the isotopic fractionation between the average stream composition and the calculated $\delta^{11}B$ of the secondary phases is close to 20‰. This value is strikingly similar to the isotopic fractionation required by the flow-through model (Eq. (2) and Fig. 6), strengthening the idea that boron isotope geochemistry at Shale Hills is predominantly controlled by inorganic processes. It is interesting to note that in earlier isotopic studies at Shale Hills (Yesavage et al., 2012; Ma et al., 2015), mass balance on Mg and Fe isotopic systems also led to the inference that there was a pool of particles that had not been sampled (other than one deep sediment sample by Ma et al. (2015)) and a flux of material that had not been analyzed in sampling strategies.

According to the current experimental and observational knowledge of boron isotopic fractionation during water rock interactions (e.g., Palmer et al., 1987; Rose et al., 2000; Lemarchand et al., 2007; Gaillardet and Lemarchand, 2018), we propose that the creation of such light material can only occur through B-coprecipitation in clays or as coatings precipitated on primary clay surfaces. From an isotopic point of view, the few available studies indicate that the secondary weathering solid becomes enriched in ^{10}B at pH values between 6 and 8. Diagenetic studies also suggest that a significant amount of boron (up to 100 ppm) can be incorporated into clays depending on the pH, partition coefficient, and boron content of the precipitating solution, though similar studies at typical soil temperatures are lacking (Williams et al., 2001; Williams and Hervig, 2005). If we use the observed high temperature (> 1000 °C) linear relationship with mineral-water B isotope fractionation (Williams et al., 2001) and extrapolate it to 25 °C it is in good agreement with the value inferred from our flow-through model at Shale Hills (Section 4.1.3). Given that adsorption or coprecipitation of boron in Fe-oxides (goethite) at natural pH ranges results in isotopic fractionation values (~ 40‰; Lemarchand et al., 2007) that are too elevated to explain the data at Shale Hills, we suggest that boron re-incorporation into clays better explains the $\delta^{11}B$ measured in the dissolved load as well as the $\delta^{11}B$ of the missing pool.

These conclusions based on boron isotopes and fluxes are consistent with the recent findings of a particle transport study at Shale Hills by Kim et al. (2018). In this study, the authors sampled river suspended sediments during flood events at Shale Hills and showed that depending upon the water flowpaths in the catchment, the chemistry of particulate material was variable, affected by grain size, shape and density. Particles transported during high discharge events appeared to be enriched in Al, Mg or K, similar to the water dispersible colloids isolated by leaching soil samples at Shale Hills (Bern and Yesavage, 2018). Groundwater may also transport significant quantities of such fine particles as scanning electron microscopic analysis of particulate matter in the groundwater at Shale Hills revealed a mineral composition of illite, vermiculite, chlorite and kaolinite (Herndon et al., 2018). These particulate material pools may all represent the exported solid ^{10}B-enriched material (B was not measured on any of these samples). When Al or Mg concentrations measured on the river sediments in this study (Table 2) are compared to those investigated by Kim et al. (2018), it appears that the sediments analyzed here for $\delta^{11}B$ have lower Al and Mg than those measured by Kim et al. (2018). Thus, sediments analyzed here are probably not representative of the material transported during flood events. During flood events, particles may be mobilized out of deep bedrock fractures.

We must, however, underscore that these measurements of stream and particle fluxes (Kim et al., 2018) were far too low (0.1 mol B $ha^{-1}y^{-1}$; using a B concentration of 60 ppm) to support the estimated solid B export required to close the mass balance (~2.4 mol B $ha^{-1}y^{-1}$). Therefore, it is difficult to imagine that the missing B flux is transported during the flood events based on today's observations. One possibility, as suggested by Kim

et al. (2018), is that a significant portion of particles is transported out of the catchment by groundwater and not by the stream. This could explain our missing pool of B if these groundwater-transported particles are carrying the missing ^{10}B. Thus, one hypothesis is that "missing" light B particles are lost through deep groundwater export from the catchment that we have not sampled. A second hypothesis is that the missing boron was lost in the past in proportions higher than are being lost today. Similarly, Ma et al. (2015) argued that greater particle loss occurred in the past from Shale Hills in order to explain the observations of Mg isotopes in the system. They invoked possible transport during periglacial conditions to explain a missing heavy Mg isotope reservoir. A similar explanation could apply to boron isotopes.

The observation that multiple isotopic systems (e.g., B, Mg, Fe) in this shale-rich system point to a missing pool suggests a fundamental gap in knowledge of how shale systems weather. Here, studies of these isotopic systems across shale catchments of varying age and climatic histories, where erosion rates have been constrained, could reveal fractionation and transport processes key to understanding this particle flux.

4.4. Implications

Findings from Shale Hills point to a critical need to quantify the isotopic composition and reservoirs of B in vegetation because significant variation in fractionation can occur between roots, wood, and leaves (Cividini et al., 2010; Geilert et al., 2019). Paying particular attention to these compartments and how they break down and are released, especially when combined with Li isotopes that are solely dictated by mineral dissolution, would help illuminate the controls on weathering fluxes and the sensitivity of the critical zone to changes in biotic and abiotic processes. Our data also offer yet another example where the simple flow-through model best predicts isotopic composition. This model is consistent with water chemistry controlled by B released from dissolution of primary minerals keeping pace with B incorporation into secondary phases. This study gives an explanation for the ^{11}B rich nature of continental waters that are discharged to the ocean. We predict that the extent of clay formation on lands, and thus weathering regimes, will have a consequence in terms of B isotopic composition of the ocean, given the fact that rivers are the main driver of ocean $\delta^{11}B$ (Lemarchand et al., 2000).

5. Conclusion

Boron concentrations and isotopes are a powerful proxy for elucidating the control of chemical weathering, sorption processes, and vegetation cycling on mass fluxes in shale catchments. The solid (i.e., particulate, soil, and bedrock) and solute (i.e., precipitation, stream water, and groundwater) boron concentrations and isotopes and results from the flow-through model revealed that the stream is dominated by B inputs from water-rock interactions including mineral dissolution and B incorporation into secondary minerals. When paired with geochemical modeling and past observations, we infer the largest proportion of B is released from chlorite dissolution in the near surface soils and regolith, and that light B is preferentially incorporated or co-precipitated on to mobile clay particles. Conversely, the release of boron from the vegetation appeared to have a limited influence. Mass balance calculations at the watershed scale showed that a pool of boron with low $\delta^{11}B$ signature is missing from our sampled pools. The isotopic signature of this pool argues for a reservoir of boron related to secondary weathering products, preferentially adsorbed or co-precipitated on clay minerals. If river suspended sediments probably contain such a pool of light boron, their current flux is not elevated enough to close the mass budget of boron isotopes at the considered timescale. We propose two hypotheses to explain the *open* boron mass budget at Shale Hills: 1) a significant portion of the particles carrying the missing ^{10}B are stored in deeper groundwater and transported by groundwater and not by the stream, and are not captured by our current sampling design and; 2) the production and export of boron is not operating at steady state in the catchment (i.e., there is no net long-term storage of boron in the system) suggesting that the missing boron has been lost in the past in proportions higher than are being lost today. Altogether, boron isotope systematics at Shale Hills confirm the conclusions reached by other isotopes in this shale system. Thus, revealing the timing and flux of the light boron pool at the small watershed scale, where more compartments can be measured and under longer timescales, may be critical for understanding riverine fluxes and their controls on the oceanic composition of boron.

Declaration of competing interest

The authors declare that they have no known competing financial interests or personal relationships that could have appeared to influence the work reported in this paper.

Acknowledgements

This work was facilitated by NSF Critical Zone Observatory program grants to SLB (EAR 12-39285, EAR 13-31726). Parts of this work were also supported by IPGP multidisciplinary program PARI, and by Paris–IdF region SESAME Grant no. 12015908. JN was founded by the French Ministry of higher Education and Institut Universitaire de France. This research was conducted in Penn State's Stone Valley Forest, which is supported and managed by the Penn State's Forestland Management Office in the College of Agricultural Sciences. We thank Lin Ma, Lixin Jin, Nicole West, Julien Bouchez and Damien Lemarchand for discussion.

Appendix A. Supplementary data

Supplementary data to this article can be found online at https://doi.org/10.1016/j.chemgeo.2020.119900.

References

Bern, C.R., Yesavage, T., 2018. Dual-phase mass balance modeling of small mineral particle losses from sedimentary rock-derived soils. Chem. Geol. 476, 441–455.
Blevins, D.G., Lukaszewski, K.M., 1998. Boron in plant structure and function. Annu. Rev. Plant Biol. 49 (1), 481–500.
Bouchez, J., Von Blanckenburg, F., Schuessler, J.A., 2013. Modeling novel stable isotope ratios in the weathering zone. Am. J. Sci. 313 (4), 267–308.
Brantley, S.L., Holleran, M.E., Jin, L., Bazilevskaya, E., 2013. Probing deep weathering in the Shale Hills Critical Zone Observatory, Pennsylvania (USA): the hypothesis of nested chemical reaction fronts in the subsurface. Earth Surf. Process. Landf. 38 (11), 1280–1298.
Brantley, S.L., Lebedeva, M.I., Balashov, V.N., Singha, K., Sullivan, P.L., Stinchcomb, G., 2017. Toward a conceptual model relating chemical reaction fronts to water flow paths in hills. Geomorphology 277, 100–117.
Brantley, S.L., White, T., West, N., Williams, J.Z., Forsythe, B., Shapich, D., ... Herndon, E., 2018. Susquehanna Shale Hills Critical Zone Observatory: Shale Hills in the context of Shaver's Creek watershed. Vadose Zone Journal 17 (1).
Broadley, M., Brown, P., Cakmak, I., Rengel, Z., Zhao, F., 2012. Function of nutrients: micronutrients. In: Marschner's Mineral Nutrition of Higher Plants. Academic Press, pp. 191–248.
Brown, P.H., Bellaloui, N., Wimmer, M.A., Bassil, E.S., Ruiz, J., Hu, H., ... Römheld, V., 2002. Boron in plant biology. Plant biology 4 (02), 205–223.
Casanova, J., Négrel, P., Kloppmann, W., Aranyossy, J.F., 2001. Origin of deep saline groundwaters in the Vienne granitic rocks (France): constraints inferred from boron and strontium isotopes. Geofluids 1 (2), 91–101.
Catanzaro, E.J., Champion, C.E., Garner, E.L., Malinenko, G., Sappenfeld, K.M., Shields, W.R., 1970. Boric acid, isotopic, and assay standard reference materials. US National Bureau of Standards Special Publication 260, 17–70.
Chetelat, B., Gaillardet, J., Freydier, R., Négrel, P., 2005. Boron isotopes in precipitation: experimental constraints and field evidence from French Guiana. Earth Planet. Sci. Lett. 235 (1–2), 16–30.
Chetelat, B., Gaillardet, J., Freydier, R., 2009a. Use of B isotopes as a tracer of anthropogenic emissions in the atmosphere of Paris, France. Appl. Geochem. 24 (5), 810–820.
Chetelat, B., Liu, C.Q., Gaillardet, J., Wang, Q.L., Zhao, Z.Q., Liang, C.S., Xiao, Y.K., 2009b. Boron isotopes geochemistry of the Changjiang basin rivers. Geochim. Cosmochim. Acta 73 (20), 6084–6097.
Cividini, D., Lemarchand, D., Chabaux, F., Boutin, R., Pierret, M.C., 2010. From biological to lithological control of the B geochemical cycle in a forest watershed (Strengbach, Vosges). Geochim. Cosmochim. Acta 74 (11), 3143–3163.
Cotter, E., Inners, J.D., Sevon, W., 1986. Silurian stratigraphy and sedimentology in the

Huntingdon County area. In: Guidebook for the 51st Annual Field Conference of Pennsylvania Geologists, Selected Geology of Bedford and Huntingdon Counties: Field Conference of Pennsylvania Geologists, Bureau of Topographic and Geologic Survey, pp. 27–39.
Davidson, C.I., Phalen, R.F., Solomon, P.A., 2005. Airborne particulate matter and human health: a review. Aerosol Sci. Technol. 39 (8), 737–749.
Dellinger, M., Gaillardet, J., Bouchez, J., Calmels, D., Louvat, P., Dosseto, A., ... Maurice, L., 2015. Riverine Li isotope fractionation in the Amazon River basin controlled by the weathering regimes. Geochimica et Cosmochimica Acta 164, 71–93.
Duffy, C., 2012. CZO Dataset :Shale Hills- Streamflow/Discharge(2006-2012)- Shale Hills stream/Discharge Data. Tec. https://scholar.google.com/scholar?hl=en&as_sdt=0%2C5&q=Boron+in+the+weathering+environment.+In+%3A+Boron+Isotopes.+&btnG=hnical (report).
Duffy, C., 2013. CZO Dataset: Shale Hills- Precipitation (2006–2013). Technical Report.
Flueckinger, L.A., 1969. Geology of a Portion of the Allensville Quadrangle, Centre and Huntingdon Counties, Pennsylvania. Commonwealth of Pennsylvania, State Planning Board, Bureau of Topographic and Geologic Survey.
Gaillardet, J., Lemarchand, D., 2018. Boron in the weathering environment. In: Marschall, H., Foster, G. (Eds.), Boron Isotopes. Springer International Publishing, Cham, pp. 163–188.
Geilert, S., Vogl, J., Rosner, M., Voerkelius, S., Eichert, T., 2015. Boron isotope fractionation in bell pepper. Mass Spectrometry & Purification Techniques 1 (101).
Geilert, S., Vogl, J., Rosner, M., Eichert, T., 2019. Boron isotope variability related to boron speciation (change during uptake and transport) in bell pepper plants and SI traceable n (11B)/n (10B) ratios for plant reference materials. Rapid Commun. Mass Spectrom. 33 (13), 1137–1147.
Gu, X., Mavko, G., Ma, L., Oakley, D., Accardo, N., Carr, B.J., Nyblade, A.A., Brantley, S.L., 2020. Seismic refraction documents clay reactions and possible CO_2 production under a ridge and valley landscape. Proc. Natl. Acad. Sci. 117 (32), 18991–18997.
Hasenmueller, E.A., Gu, X., Weitzman, J.N., Adams, T.S., Stinchcomb, G.E., Eissenstat, D.M., Drohan, P.J., Brantley, S.L., Kaye, J.P., 2017. Weathering of rock to regolith: the activity of deep roots in bedrock fractures. Geoderma 300, 11–31.
Herndon, E.M., Dere, A.L., Sullivan, P.L., Norris, D., Reynolds, B., Brantley, S.L., 2015a. Biotic controls on solute distribution and transport in headwater catchments. Hydrol. Earth Syst. Sci. 213.
Herndon, E.M., Jin, L., Andrews, D.M., Eissenstat, D.M., Brantley, S.L., 2015b. Importance of vegetation for manganese cycling in temperate forested watersheds. Glob. Biogeochem. Cycles 29 (2), 160–174.
Herndon, E.M., Steinhoefel, G., Dere, A.L., Sullivan, P.L., 2018. Perennial flow through convergent hillslopes explains chemodynamic solute behavior in a shale headwater catchment. Chem. Geol. 493, 413–425.
Hu, Z., Gao, S., 2008. Upper crustal abundances of trace elements: a revision and update. Chem. Geol. 253 (3–4), 205–221.
Jin, L., Ravella, R., Ketchum, B., Bierman, P.R., Heaney, P., White, T., Brantley, S.L., 2010. Mineral weathering and elemental transport during hillslope evolution at the Susquehanna/Shale Hills Critical Zone Observatory. Geochim. Cosmochim. Acta 74 (13), 3669–3691.
Jin, L., Andrews, D.M., Holmes, G.H., Lin, H., Brantley, S.L., 2011. Opening the "black box": water chemistry reveals hydrological controls on weathering in the Susquehanna Shale Hills Critical Zone Observatory. Vadose Zone J. 10 (3), 928–942.
Jin, L., Ogrinc, N., Yesavage, T., Hasenmueller, E.A., Ma, L., Sullivan, P.L., ... Brantley, S. L., 2014. The CO_2 consumption potential during gray shale weathering: insights from the evolution of carbon isotopes in the Susquehanna Shale Hills critical zone observatory. Geochimica et Cosmochimica Acta 142, 260–280.
Kim, H., Gu, X., Brantley, S.L., 2018. Particle fluxes in groundwater change subsurface shale rock chemistry over geologic time. Earth Planet. Sci. Lett. 500, 180–191.
Lemarchand, D., Gaillardet, J., 2006. Transient features of the erosion of shales in the Mackenzie basin (Canada), evidences from boron isotopes. Earth Planet. Sci. Lett. 245 (1–2), 174–189.
Lemarchand, D., Gaillardet, J., Lewin, E., Allegre, C.J., 2000. The influence of rivers on marine boron isotopes and implications for reconstructing past ocean pH. Nature 408 (6815), 951–954.
Lemarchand, E., Schott, J., Gaillardet, J., 2007. How surface complexes impact boron isotope fractionation: evidence from Fe and Mn oxides sorption experiments. Earth Planet. Sci. Lett. 260 (1–2), 277–296.
Lemarchand, D., Cividini, D., Turpault, M.P., Chabaux, F., 2012. Boron isotopes in different grain size fractions: Exploring past and present water–rock interactions from two soil profiles (Strengbach, Vosges Mountains). Geochim. Cosmochim. Acta 98, 78–93.
Lemarchand, D., Jacobson, A.D., Cividini, D., Chabaux, F., 2015. The major ion, 87Sr/86Sr, and δ11B geochemistry of groundwater in the Wyodak-Anderson coal bed aquifer (Powder River Basin, Wyoming, USA). Compt. Rendus Geosci. 347 (7–8), 348–357.
Li, L., Bao, C., Sullivan, P.L., Brantley, S., Shi, Y., Duffy, C., 2017. Understanding watershed hydrogeochemistry: 2. Synchronized hydrological and geochemical processes drive stream chemostatic behavior. Water Resources Research 53 (3), 2346–2367.
Lin, H., 2006. Temporal stability of soil moisture spatial pattern and subsurface preferential flow pathways in the Shale Hills Catchment. Vadose Zone J. 5 (1), 317–340.
Louvat, P., Bouchez, J., Paris, G., 2010. MC-ICP-MS isotope measurements with direct injection nebulisation (d-DIHEN): optimisation and application to boron in seawater and carbonate samples. Geostand. Geoanal. Res. 35 (1), 75–88.
Louvat, P., Gaillardet, J., Paris, G., Dessert, C., 2011. Boron isotope ratios of surface waters in Guadeloupe, Lesser Antilles. Appl. Geochem. 26, S76–S79.
Louvat, P., Gayer, E., Gaillardet, J., 2014a. Boron behavior in the rivers of Réunion island, inferred from boron isotope ratios and concentrations of major and trace elements. Procedia Earth and Planetary Science 10, 231–237.
Louvat, P., Moureau, J., Paris, G., Bouchez, J., Noireaux, J., Gaillardet, J., 2014b. A fully automated direct injection nebulizer (d-DIHEN) for MC-ICP-MS isotope analysis: application to boron isotope ratio measurements. J. Anal. At. Spectrom. 29 (9), 1698–1707.
Ma, L., Chabaux, F., Pelt, E., Blaes, E., Jin, L., Brantley, S., 2010. Regolith production rates calculated with uranium-series isotopes at Susquehanna/Shale Hills Critical Zone Observatory. Earth Planet. Sci. Lett. 297 (1–2), 211–225.
Ma, L., Jin, L., Brantley, S.L., 2011. Geochemical behaviors of different element groups during shale weathering at the Susquehanna/Shale Hills Critical Zone Observatory. Appl. Geochem. 26, S89–S93.
Ma, L., Chabaux, F., West, N., Kirby, E., Jin, L., Brantley, S., 2013. Regolith production and transport in the Susquehanna Shale Hills Critical Zone Observatory, part 1: insights from U-series isotopes. Journal of Geophysical Research: Earth Surface 118 (2), 722–740.
Ma, L., Teng, F.Z., Jin, L., Ke, S., Yang, W., Gu, H.O., Brantley, S.L., 2015. Magnesium isotope fractionation during shale weathering in the Shale Hills Critical Zone Observatory: Accumulation of light Mg isotopes in soils by clay mineral transformation. Chem. Geol. 397, 37–50.
Mather, J.D., Porteous, N.C., 2001. The geochemistry of boron and its isotopes in groundwaters from marine and non-marine sandstone aquifers. Appl. Geochem. 16 (7–8), 821–834.
Michel, A., Noireaux, J., Tharaud, M., 2015. Determination of boron concentration in geochemical reference materials extracted by pyrohydrolysis and measured by ICP-MS. Geostand. Geoanal. Res. 39, 489–495.
Millot, R., Petelet-Giraud, E., Guerrot, C., Négrel, P., 2010a. Multi-isotopic composition (δ7Li–δ11B–δD–δ18O) of rainwaters in France: Origin and spatio-temporal characterization. Appl. Geochem. 25 (10), 1510–1524.
Millot, R., Vigier, N., Gaillardet, J., 2010b. Behaviour of lithium and its isotopes during weathering in the Mackenzie Basin, Canada. Geochim. Cosmochim. Acta 74 (14), 3897–3912.
Noireaux, J., Gaillardet, J., Sullivan, P.L., Brantley, S.L., 2014. Boron isotope fractionation in soils at Shale Hills CZO. Procedia Earth and Planetary Science 10, 218–222.
Opfergelt, S., Georg, R.B., Delvaux, B., Cabidoche, Y.M., Burton, K.W., Halliday, A.N., 2012. Mechanisms of magnesium isotope fractionation in volcanic soil weathering sequences, Guadeloupe. Earth Planet. Sci. Lett. 341, 176–185.
Palmer, M.R., Spivack, A.J., Edmond, J.M., 1987. Temperature and pH controls over isotopic fractionation during adsorption of boron on marine clay. Geochim. Cosmochim. Acta 51 (9), 2319–2323.
Paris, G., Bartolini, A., Donnadieu, Y., Beaumont, V., Gaillardet, J., 2010. Investigating boron isotopes in a middle Jurassic micritic sequence: primary vs. diagenetic signal. Chem. Geol. 275 (3–4), 117–126.
Park, H., Schlesinger, W.H., 2002. Global biogeochemical cycle of boron. Glob. Biogeochem. Cycles 16 (4), 20–21.
Pennisi, M., Bianchini, G., Muti, A., Kloppmann, W., Gonfiantini, R., 2006. Behaviour of boron and strontium isotopes in groundwater–aquifer interactions in the Cornia Plain (Tuscany, Italy). Appl. Geochem. 21 (7), 1169–1183.
Power, P.P., Woods, W.G., 1997. The chemistry of boron and its speciation in plants. Plant Soil 193 (1–2), 1–13.
Romer, R.L., Meixner, A., Hahne, K., 2014. Lithium and boron isotopic composition of sedimentary rocks—the role of source history and depositional environment: a 250 Ma record from the Cadomian orogeny to the Variscan orogeny. Gondwana Res. 26 (3–4), 1093–1110.
Rose, E.F., Chaussidon, M., France-Lanord, C., 2000. Fractionation of boron isotopes during erosion processes: the example of Himalayan rivers. Geochim. Cosmochim. Acta 64 (3), 397–408.
Rose-Koga, E.F., Sheppard, S.M.F., Chaussidon, M., Carignan, J., 2006. Boron isotopic composition of atmospheric precipitations and liquid–vapour fractionations. Geochim. Cosmochim. Acta 70 (7), 1603–1615.
Roux, P., Turpault, M.P., Kirchen, G., Redon, P.O., Lemarchand, D., 2017. Boron dissolved and particulate atmospheric inputs to a forest ecosystem (Northeastern France). Environmental Science & Technology 51 (24), 14038–14046.
Ruhl, L.S., Dwyer, G.S., Hsu-Kim, H., Hower, J.C., Vengosh, A., 2014. Boron and strontium isotopic characterization of coal combustion residuals: validation of new environmental tracers. Environmental Science & Technology 48 (24), 14790–14798.
Schmitt, A.D., Vigier, N., Lemarchand, D., Millot, R., Stille, P., Chabaux, F., 2012. Processes controlling the stable isotope compositions of Li, B, Mg and Ca in plants, soils and waters: a review. Compt. Rendus Geosci. 344 (11–12), 704–722.
Smith, L.A., 2013. Aboveground Carbon Distribution across a Temperate Watershed. Master Thesis. The Pennsylvania State University.
Spivack, A.J., Palmer, M.R., Edmond, J.M., 1987. The sedimentary cycle of the boron isotopes. Geochim. Cosmochim. Acta 51 (7), 1939–1949.
Sullivan, P.L., Ma, L., West, N., Jin, L., Karwan, D.L., Noireaux, J., ... Derry, L.A., 2016a. CZ-tope at Susquehanna Shale Hills CZO: Synthesizing multiple isotope proxies to elucidate Critical Zone processes across timescales in a temperate forested landscape. Chemical Geology 445, 103–119.
Sullivan, P.L., Hynek, S.A., Gu, X., Singha, K., White, T., West, N., ... Brantley, S.L., 2016b. Oxidative dissolution under the channel leads geomorphological evolution at the Shale Hills catchment. American Journal of Science 316 (10), 981–1026.
Sullivan, P.L., Goddéris, Y., Shi, Y., Gu, X., Schott, J., Hasenmueller, E.A., ... Brantley, S.L., 2019. Exploring the effect of aspect to inform future earthcasts of climate-driven changes in weathering of shale. Journal of Geophysical Research: Earth Surface. 124.
Thomas, E.M., Lin, H., Duffy, C.J., Sullivan, P.L., Holmes, G.H., Brantley, S.L., Jin, L., 2013. Spatiotemporal patterns of water stable isotope compositions at the Shale Hills Critical Zone Observatory: Linkages to subsurface hydrologic processes. Vadose Zone J. 12 (4).
Tonarini, S., Pennisi, M., Leeman, W.P., 1997. Precise boron isotopic analysis of complex

silicate (rock) samples using alkali carbonate fusion and ion-exchange separation. Chem. Geol. 142 (1–2), 129–137.
Vengosh, A., Heumann, K.G., Juraske, S., Kasher, R., 1994. Boron isotope application for tracing sources of contamination in groundwater. Environmental Science & Technology 28 (11), 1968–1974.
Vogl, J., Rosner, M., 2011. Production and Certification of a Unique Set of Isotope and Delta Reference Materials for Boron Isotope Determination in Geochemical, Environmental and Industrial Materials. Geost. Geoanal. Res 36, 161–175.
Wei, G., Jingxian, W., Ying, L., Ting, K., Zhongyuan, R., Jinlong, M., Yigang, X., 2013. Measurement on high-precision boron isotope of silicate materials by a single column purification method and MC-ICP-MS. J. Anal. At. Spectrom 28, 606. https://doi.org/10.1039/c3ja30333k.
Weitzman, J.N., Kaye, J.P., 2018. Nitrogen budget and topographic controls on nitrous oxide in a shale-based watershed. Journal of Geophysical Research: Biogeosciences 123 (6), 1888–1908.
West, N., Kirby, E., Bierman, P., Slingerland, R., Ma, L., Rood, D., Brantley, S., 2013. Regolith production and transport at the Susquehanna Shale Hills Critical Zone Observatory, part 2: insights from meteoric 10Be. Journal of Geophysical Research: Earth Surface 118 (3), 1877–1896.
Williams, L.B., Hervig, R.L., 2005. Lithium and boron isotopes in illite-smectite: the importance of crystal size. Geochim. Cosmochim. Acta 69 (24), 5705–5716.
Williams, L.B., Hervig, R.L., Holloway, J.R., Hutcheon, I., 2001. Boron isotope geochemistry during diagenesis. Part I. Experimental determination of fractionation during illitization of smectite. Geochim. Cosmochim. Acta 65 (11), 1769–1782.
Yesavage, T., Fantle, M.S., Vervoort, J., Mathur, R., Jin, L., Liermann, L.J., Brantley, S.L., 2012. Fe cycling in the Shale Hills Critical Zone Observatory, Pennsylvania: an analysis of biogeochemical weathering and Fe isotope fractionation. Geochim. Cosmochim. Acta 99, 18–38.
Zhao, Z.Q., Liu, C.Q., 2010. Anthropogenic inputs of boron into urban atmosphere: evidence from boron isotopes of precipitations in Guiyang City, China. Atmos. Environ. 44 (34), 4165–4171.